

---

# Impaired catabolism of free oligosaccharides due to *MAN2C1* variants causes a neurodevelopmental disorder

## Authors

Nuno Maia, Sven Potelle, Hamide Yildirim, ...,  
Paula Jorge, Anna C. Jansen, François Foulquier

## Correspondence

[francois.foulquier@univ-lille.fr](mailto:francois.foulquier@univ-lille.fr) (F.F.),  
[anna.jansen@vub.be](mailto:anna.jansen@vub.be) (A.C.J.)



# Impaired catabolism of free oligosaccharides due to *MAN2C1* variants causes a neurodevelopmental disorder

Nuno Maia,<sup>1,2,23</sup> Sven Potelle,<sup>3,4,23</sup> Hamide Yildirim,<sup>5,23</sup> Sandrine Duvet,<sup>6</sup> Shyam K. Akula,<sup>7,8,9,10,11</sup> Celine Schulz,<sup>6</sup> Elsa Wiame,<sup>3,4</sup> Alexander Gheldof,<sup>12,13</sup> Katherine O’Kane,<sup>7,8,9,10,11</sup> Abbe Lai,<sup>7,8,9,10,11</sup> Karen Sermon,<sup>13</sup> Maïa Proisy,<sup>14</sup> Philippe Loget,<sup>15</sup> Tania Attié-Bitach,<sup>16,17</sup> Chloé Quelin,<sup>18</sup> Ana Maria Fortuna,<sup>1,2</sup> Ana Rita Soares,<sup>1</sup> Arjan P.M. de Brouwer,<sup>19</sup> Emile Van Schaftingen,<sup>3,4</sup> Marie-Cécile Nassogne,<sup>20,21</sup> Christopher A. Walsh,<sup>7,8,9,10,11</sup> Katrien Stouffs,<sup>12,13</sup> Paula Jorge,<sup>1,2,24</sup> Anna C. Jansen,<sup>5,22,24,\*</sup> and François Foulquier<sup>6,24,\*</sup>

## Summary

Free oligosaccharides (fOSs) are soluble oligosaccharide species generated during N-glycosylation of proteins. Although little is known about fOS metabolism, the recent identification of NGLY1 deficiency, a congenital disorder of deglycosylation (CDDG) caused by loss of function of an enzyme involved in fOS metabolism, has elicited increased interest in fOS processing. The catabolism of fOSs has been linked to the activity of a specific cytosolic mannosidase, *MAN2C1*, which cleaves  $\alpha$ 1,2-,  $\alpha$ 1,3-, and  $\alpha$ 1,6-mannose residues. In this study, we report the clinical, biochemical, and molecular features of six individuals, including two fetuses, with bi-allelic pathogenic variants in *MAN2C1*; the individuals are from four different families. These individuals exhibit dysmorphic facial features, congenital anomalies such as tongue hamartoma, variable degrees of intellectual disability, and brain anomalies including polymicrogyria, interhemispheric cysts, hypothalamic hamartoma, callosal anomalies, and hypoplasia of brainstem and cerebellar vermis. Complementation experiments with isogenic *MAN2C1*-KO HAP1 cells confirm the pathogenicity of three of the identified *MAN2C1* variants. We further demonstrate that *MAN2C1* variants lead to accumulation and delay in the processing of fOSs in proband-derived cells. These results emphasize the involvement of *MAN2C1* in human neurodevelopmental disease and the importance of fOS catabolism.

## Introduction

N-linked glycosylation is a ubiquitous posttranslational modification of proteins found in all eukaryotes that results from the transfer of an oligosaccharide on specific asparagine residues followed by its processing.<sup>1</sup> This N-glycan serves several crucial functions in the folding, trafficking, and degradation of glycoproteins but also in cell signaling and intercellular communication.<sup>2</sup> This process originates at the endoplasmic reticulum (ER) membrane with the synthesis of an oligosaccharide Glc<sub>3</sub>Man<sub>9</sub>GlcNAc<sub>2</sub> precursor linked to a lipid carrier, dolichol pyrophosphate (Figure 1).

<sup>1</sup> The membrane oligosaccharyltransferase (OST) complex catalyzes the transfer of this oligosaccharide during the

translation and translocation of the protein.<sup>3</sup> The importance of this pathway has been illustrated with the identification of defects in genes involved in N-linked oligosaccharide biosynthesis and leading to congenital disorders of glycosylation (CDGs).<sup>4–6</sup>

Interestingly, the N-glycosylation process is accompanied by the release of free oligosaccharides (fOSs) both in the cytoplasm and the ER lumen.<sup>7</sup> Endoplasmic-reticulum-associated protein degradation (ERAD) has been shown in both yeast and mammals to generate fOSs (ERAD pathway, Figure 1). Newly synthesized glycoproteins that fail to fold correctly within the ER are translocated from the ER to the cytosol for proteasomal degradation. However, this degradation can only take place if N-glycans are removed

<sup>1</sup>Centro de Genética Médica Doutor Jacinto Magalhães, Centro Hospitalar Universitário do Porto, 4050-466 Porto, Portugal; <sup>2</sup>Unit for Multidisciplinary Research in Biomedicine and Laboratory for Integrative and Translational Research in Population Health, Institute of Biomedical Sciences Abel Salazar, University of Porto, 4050-313 Porto, Portugal; <sup>3</sup>Laboratory of Physiological Chemistry, de Duve Institute, 1200 Brussels, Belgium; <sup>4</sup>WELBIO, 1200 Brussels, Belgium; <sup>5</sup>Neurogenetics Research Group, Reproduction Genetics and Regenerative Medicine Research Cluster, Vrije Universiteit Brussel, 1090 Brussels, Belgium; <sup>6</sup>Univ. Lille, CNRS, UMR 8576-UGSF-Unit. de Glycobiologie Structurale et Fonctionnelle, 59000 Lille, France; <sup>7</sup>Division of Genetics and Genomics, Boston Children’s Hospital, Boston, MA 02115, USA; <sup>8</sup>Howard Hughes Medical Institute, Boston, MA 02115, USA; <sup>9</sup>Broad Institute of MIT and Harvard, Boston, MA 02115, USA; <sup>10</sup>Manton Center for Orphan Disease Research, Boston, MA 02115, USA; <sup>11</sup>Harvard Medical School, Boston, MA 02115, USA; <sup>12</sup>Centre for Medical Genetics, UZ Brussel, 1090 Brussels, Belgium; <sup>13</sup>Reproduction and Genetics Research Group, Vrije Universiteit Brussel, 1090 Brussels, Belgium; <sup>14</sup>CHU Brest, Radiology Department, Brest University, 29609 Brest Cedex, France; <sup>15</sup>Department of Pathology, Rennes University Hospital, 35000 Rennes, France; <sup>16</sup>APHP, Embryofœtopathologie, Service d’Histologie-Embryologie-Cytogénétique, Hôpital Universitaire Necker-Enfants Malades, 75015 Paris, France; <sup>17</sup>Université de Paris, Imagine Institute, INSERM UMR 1163, 75015 Paris, France; <sup>18</sup>Clinical Genetics Department, Rennes University Hospital, 35000 Rennes, France; <sup>19</sup>Department of Human Genetics, Donders Institute for Brain, Cognition and Behavior, Radboud University Medical Center, 6500 Nijmegen, the Netherlands; <sup>20</sup>Department of Pediatric Neurology, Cliniques Universitaires Saint-Luc, UCLouvain, 1200 Brussels, Belgium; <sup>21</sup>Institute Of Neuroscience, Clinical Neuroscience, UCLouvain, 1200 Brussels, Belgium; <sup>22</sup>Pediatric Neurology Unit, Department of Pediatrics, UZ Brussel, 1090 Brussels, Belgium

<sup>23</sup>These authors contributed equally

<sup>24</sup>These authors contributed equally

\*Correspondence: francois.foulquier@univ-lille.fr (F.F.), anna.jansen@vub.be (A.C.J.)

<https://doi.org/10.1016/j.ajhg.2021.12.010>

© 2022 The Authors. This is an open access article under the CC BY-NC-ND license (<http://creativecommons.org/licenses/by-nc-nd/4.0/>).



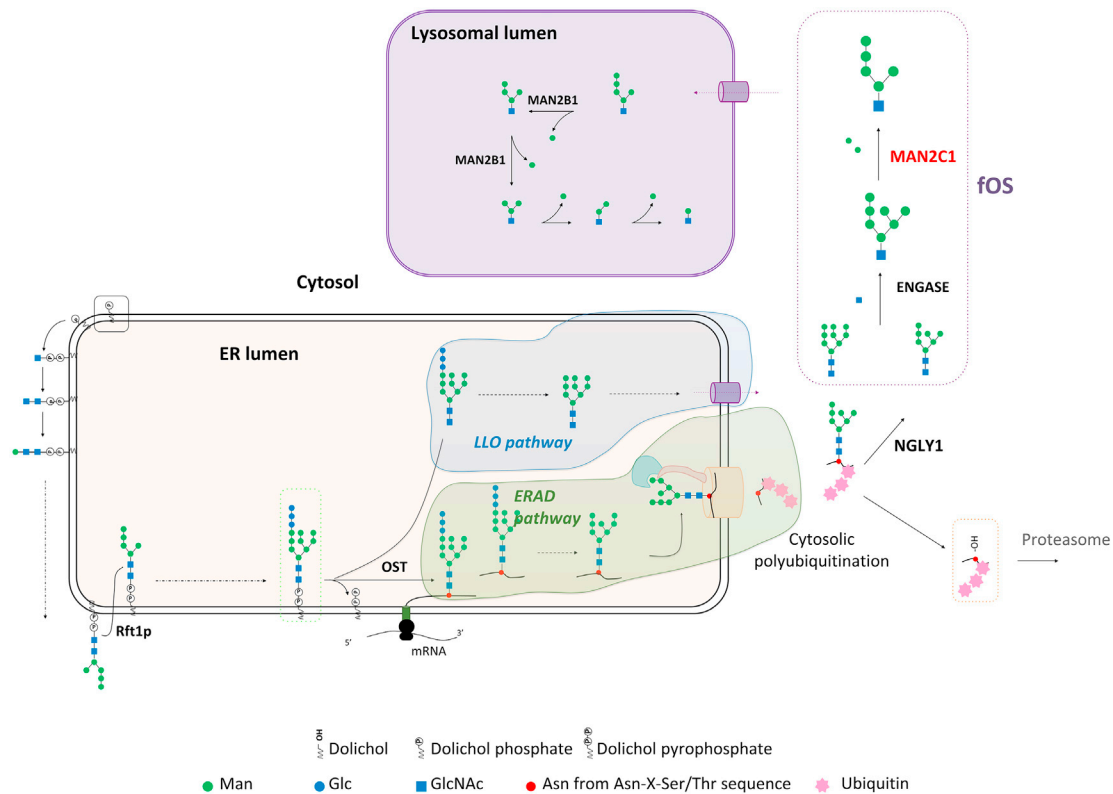


**Figure 1. Metabolism of free oligosaccharides (fOS) in mammalian cells**

fOSs are either generated during the ERAD pathway following the action of NGLY1 and/or via the hydrolysis of lipid-linked oligosaccharide by OST (LLO pathway). Once in the cytosol, ENGase cleaves the chitobiose core to form Gn1 fOSs with a single GlcNAc at their reducing end. These fOS species are then processed by the cytosolic  $\alpha$ -mannosidase (MAN2C1) leading to the specific isomeric Man5GlcNAc1 structure. The catabolism of these species continues in the lysosomes by lysosomal  $\alpha$ - and  $\beta$ -mannosidases.

from the peptidic backbone prior to degradation. This occurs due to the cytosolic PNGase (NGLY1), which generates fOSs possessing two GlcNAc residues (fOS<sub>Gn2</sub>) at their reducing end (Figure 1).<sup>8,9</sup> These specific oligosaccharides are then further trimmed by the sequential action of ENGase that cleaves between the two sugars of the chitobiose motif-generating fOS containing only one GlcNAc residue (fOS<sub>Gn1</sub>) at the reducing end.<sup>10</sup> The second pathway involves the catalytic activity of OST on water molecules (LLO pathway, Figure 1).<sup>11</sup> This OST-dependent pathway produces fOS within the ER lumen from LLO. The resulting Glc<sub>3</sub>Man<sub>9</sub>GlcNAc<sub>2</sub> structure is then further trimmed in the ER lumen by the ER glucosidases I/II and mannosidases before being retro-translocated from the ER to the cytosol. The ER transporter involved in this process is unknown, but it is both ATP dependent and glycan-structure dependent because non-glucosylated species have been found to be preferentially transported.<sup>12,13</sup> Once inside the cytosol, these fOSs are indistinguishable from those generated by ERAD. The fate of these cytosolic fOSs is linked to the activity of the cytosolic mannosidase MAN2C1, which cleaves  $\alpha$ 1,2-,  $\alpha$ 1,3-, and  $\alpha$ 1,6-mannose residues on fOSs.<sup>14-17</sup>

MAN2C1 is located at 15q24.2 (MIM:154580) and contains 26 exons coding for 1,040 amino acid residues

(GenBank: NM\_006715.3 and NP\_006706.2), of which exons 6 to 13 encode glycoside hydrolase family 38 N-terminal domain (InterPro: IPR000602, 252–510 amino acids), exons 13 to 16 encode the glycoside hydrolase family 38 central domain (InterPro: IPR015341, 517–614 amino acids), exons 18 to 23 encode the glycoside hydrolase family 38 C-terminal domain (InterPro: IPR011682, 689–895 amino acids), and exons 24 to 26 encode the glycoside hydrolase family 38 C-terminal beta sandwich domain (InterPro: IPR041147, 955–1,031 amino acids).<sup>18</sup> Structural comparison with SpAms1 indicates that it forms a tetramer and suggests that human MAN2C1 active site nucleophile and acid/base catalyst locates at residues Asp372 and Asp463 in the glycoside hydrolase family 38 N-terminal domain.<sup>19</sup> Evolutionarily conserved, the catalytic activity is Co<sup>2+</sup> dependent and inhibited by furanose analogs.<sup>14</sup> MAN2C1 preferentially acts on Gn<sub>1</sub> rather than Gn<sub>2</sub> fOS species by converting Man<sub>7-9</sub>Gn<sub>1</sub> to Man<sub>5</sub>Gn<sub>1</sub>, the end-product of the MAN2C1 enzyme.<sup>14,17</sup> These specific Man<sub>5</sub>Gn<sub>1</sub> species are eventually transported to the lysosomes for further degradation (Figure 1).<sup>12</sup>

The importance of fOS metabolism is not understood but interest is growing since the identification of the first individual with defects in this pathway in 2012. N-glycanase 1 deficiency disorder (NGLY1-CDDG) (MIM: 615273) is a

rare congenital disorder of deglycosylation caused by a lack of NGLY1 activity.<sup>20,21</sup> The clinical phenotype of these individuals is extremely severe, mainly characterized by mild to profound intellectual disability, hypo- or alacrima, transiently elevated liver transaminases, and a complex hyperkinetic movement disorder.<sup>20</sup> The defective generation and processing of these free oligosaccharides is certainly essential in the etiology of the disease, but there is currently no clear understanding of the exact pathophysiological mechanism. To date, NGLY1 is the sole example of a defective fOS metabolism in the context of human diseases.

MAN2C1 has been implicated, beyond its specifically described role in fOS catabolism, in apoptotic signaling.<sup>22</sup> MAN2C1 suppression increased mitotic arrest and apoptosis in esophageal carcinoma cells *in vitro*, and MAN2C1 activity has been implicated in tumorigenesis of prostate cancer, although the underlying mechanisms have not been elucidated. MAN2C1 has also been shown to interact with PTEN (phosphatase and tensin homolog), inhibiting its lipid phosphatase activity.<sup>23</sup>

MAN2C1-deficient mice accumulate fOS in tissues and show biochemical and histological alterations in the central nervous system (CNS), liver, and intestine. The CNS was most severely affected and had neuronal and glial degeneration, neuronal vacuolization, and general lesions in the subcortical white matter.<sup>24</sup> Furthermore, a population-based analysis, which studied ancient haplotypes at the 15q24.2 microdeletion region, suggests that MAN2C1 variants may contribute to speech delay and intellectual disability.<sup>25</sup> To date, no other disorder or individual with pathogenic variants in MAN2C1 has been reported.

In this study, we present six individuals, including two fetuses, with bi-allelic pathogenic variants in MAN2C1; the individuals are from four different families. We then characterize the impacts of the identified missense variants on the mannosidase function of MAN2C1. Our data indicate that MAN2C1-deficient proband-derived cells accumulate fOSs. Complementation experiments with isogenic MAN2C1-KO HAP1 cells of three individuals demonstrate the pathogenicity of the identified MAN2C1 variants. These data break new ground by showing the importance of fOS metabolism and reveal the unexpected involvement of MAN2C1 in human neurodevelopmental disease.

## Material and methods

### Molecular studies

This study was performed in accordance with ethical principles for medical research outlined in the Declaration of Helsinki. Informed consent was obtained from all families. The study was approved by the research ethics board of the Centro Hospitalar Universitário do Porto (CHUPorto) REF 2015.196 (168-DEFI/157-CES) and the Commissie Medische Ethiek UZ Brussel B.U.N. 1432021000415. Individuals were gathered through GeneMatcher<sup>26</sup> following identification of bi-allelic MAN2C1 variants by exome sequencing (DNA extracted from peripheral blood). The detected variants were confirmed by Sanger sequencing via routine methodologies.

Also, siblings/parents were tested. MAN2C1 variants were numbered according to GenBank: NM\_006715.4, referring to isoform 1 (i.e., the major transcript), and annotated with the Human Genome Variation Society (HGVS) recommendations.<sup>27,28</sup> Variants' frequencies were accessed with gnomAD,<sup>29</sup> Gencode transcript: ENST00000267978. *In silico* deleteriousness, for missense variants, and spliceogenic effect predictions were determined using the following tools: (1) combined annotation-dependent depletion scoring (CADD threshold  $\geq 15$ );<sup>30</sup> (2) NNSPLICE (NNS, normal score threshold  $\geq 0.4$  for splice donor site [SDS] and splice acceptor site [SAS]);<sup>31</sup> and (3) SpliceSiteFinder-like (SSF, normal score threshold  $\geq 70$  for SDS and SAS).<sup>31</sup> Nucleotide conservation was analyzed with phyloP scores (phylogenetic p values, available as part of the PHAST package).<sup>32</sup> Protein's FASTA sequences of 12 species were obtained from Uniprot<sup>33</sup> and Ensembl Genome Browser,<sup>34</sup> and amino acid conservation analysis was performed according to the Clustal X color code<sup>35</sup> with Jalview 2 software.<sup>36</sup> Residues' physicochemical differences were determined with the Grantham distance score.<sup>37</sup> Relevant protein domains were accessed at IntroPro database.<sup>18</sup> We used the Protein Data Bank (PDB)<sup>38</sup> file 6lzl.1.A to create a homologous model for amino acid residues 67 to 1017, which are 41.6% identical to MAN2C1. MAN2C1 ortholog protein modeling was performed by Swiss Model Server,<sup>39</sup> and PyMOL Molecular Graphics System, version 2.4.2 (Schrödinger LLC, New York, NY, USA)<sup>40</sup> was used for the *in silico* mutagenesis visualization of missense variants.

RNA was obtained from fibroblasts (individual 1 and 2) via PerfectPure RNA Tissue Kit (5 PRIME, Hamburg, Germany). We use Superscript One-Step RT-PCR transcript analysis with Platinum Taq kit (Invitrogen, Carlsbad, CA, United States) to amplify the region encompassing exons 3 to 8 of MAN2C1 cDNA, using the primers cMAN2C1-3-8-F and cMAN2C1-3-8-R (Table S1), following manufacturer's instructions. PCR products were sequenced with the BigDye Terminator v3.1 cycle sequencing kit (Applied Biosystems, Foster City, CA, USA), after purification of the PCR products with Illustra exostar 1-Step, (GE Healthcare Life Sciences, Little Chalfont, UK).

### Cell lines

Fibroblasts derived from individuals with pathogenic variants in MAN2C1 were grown in Dulbecco's modified Eagle's medium (DMEM) supplemented with 10% FBS. All cell lines were maintained at 37°C and with 5% CO<sub>2</sub> in a humid atmosphere. Control, KO Man2C1, and complemented Hap1 cell lines (Horizon Discovery, Waterbeach, UK) were cultured in Iscove's modified Dulbecco's medium (IMDM) supplemented with 10% FBS (Corning, USA).

### Protein extraction and immunoblotting

Cells were washed twice with cold Dulbecco's phosphate buffer saline (1X D-PBS) before being scraped and centrifuged at 200 g during 10 min at 4°C. The supernatant was discarded and the pellet resuspended in RIPA buffer (50 mM Tris/HCl [pH 7.9], 120 mM NaCl, 0.5% NP40, 1 mM EDTA, 1 mM Na<sub>3</sub>VO<sub>4</sub>, 5 mM NaF) supplemented with protease cocktail inhibitor (Roche Diagnostics, Penzberg, Germany), mechanical lysis and incubation for 10 min followed by centrifugation at 4°C (20.000 g, 30min). Total protein concentration was assessed with Micro BCA Protein Assay Reagent kit (Thermo Fisher Scientific, Waltham, MA, USA). 20 µg of protein lysate was separated by SDS/PAGE and immunoblotted on a nitrocellulose membrane with respective antibodies. Mouse monoclonal anti-Man2C1 antibody (C-4 clone), Santa Cruz Biotechnology, USA) and monoclonal

mouse anti- $\beta$ -actin antibody ([AC-15 clone], Sigma-Aldrich-Merck) were used at a dilution of 1:500 and 1:10,000, respectively. Signals were detected with chemiluminescence reagent Pierce Pico Plus Western Blotting Substrate (Thermo Fisher Scientific, Waltham, MA, USA) and acquired with the Camera Fusion (Fusion Solo, Vilber Lourmat, Marne-la-Vallée, France).

### Metabolic and pulse-chase radiolabeling

For the pulse period, cells were first preincubated in DMEM containing 10% of dialyzed FBS (Corning, USA) and 0.5 mM of glucose before being metabolically labeled with [ $^2$ - $^3$ H] mannose (PerkinElmer, Waltham, MA, USA). For the chase period, labeled cells were washed twice and then incubated in regular medium containing 10% FBS and 25 mM glucose. After metabolic labeling, cells were washed three times with 1X D-PBS and sequential extraction and purification of oligosaccharide material were performed as described previously.<sup>6</sup> Analysis of the oligosaccharide samples was performed by high-performance liquid chromatography (HPLC) with an amino-derived Asahipak NH2P-50 4E column (250 × 4.6 mm; Shodex, Showa Denko K.K. [SDK], Tokyo, Japan).

### Plasmid constructions

Human *MAN2C1* was amplified from human skin fibroblasts cDNA via Q5 polymerase following the manufacturer's protocol. To clone the cDNA into the pEF6/V5-HisB plasmid, we used the primers EW\_MAN2C1\_His\_EcoRI\_F and EW\_MAN2C1\_NotI\_R (Table S1), respectively containing *EcoRI* and *NotI* restriction sites, to amplify human *MAN2C1*. The resulting PCR product was digested with the restriction endonucleases *EcoRI* and *NotI* and cloned into the respective *EcoRI* and *NotI* sites of the pEF6/V5-HisB plasmid. The resulting plasmid is named pEW1. To clone the cDNA into pCMV5 plasmid, we used the primers EW\_MAN2C1\_EcoRI\_F and EW\_MAN2C1\_KpnI\_R (Table S1), respectively containing *EcoRI* and *KpnI* restriction sites, to amplify the human *MAN2C1*. The resulting PCR product was digested with the restriction endonucleases *EcoRI* and *KpnI* and ligated into the respective *EcoRI* and *KpnI* sites of the pCMV5 plasmid. The resulting plasmid is named pEW2.

Site-directed mutagenesis was performed by PCR with the primers listed in Table S1. Briefly, pEW1 and pEW2 were amplified with the primers described in the list. The PCR products were digested by *DpnI* for removal of the parental plasmid and then transfected into XL1 Blue competent bacteria. Plasmid DNA from clones were extracted, purified, and sequenced. To shuttle the inserts into vectors compatible for lentiviral infection, we amplified the open reading frame of cDNA encoding wild-type, p.Gly203Arg, p.Arg768Gln, p.Cys871Ser *MAN2C1* from constructs in pEF6/V5-HisB by PCR by using Q5 polymerase (New England Biolabs) and adding flanking *XbaI*-*NotI* sites using the primers hMAN2C1\_XbaI\_FW and hMAN2C1\_NotI\_REV (Table S1). The resulting PCR products were digested with the restriction endonucleases *XbaI* and *NotI* and cloned into the respective *XbaI* and *NotI* sites of the plasmid pUB82 and pUB83. pUB82 and pUB83 are lentiviral expression vectors based on the plasmid pLVX-PURO (Clontech). In pUB82, the expression is driven by a truncated SV40 promoter that allows low levels of expression, whereas in pUB83, the expression is driven by a CMV promoter, allowing higher levels of expression.

### Recombinant lentiviruses production

Recombinant lentiviruses were produced by transiently transfecting HEK293T cells with second generation packaging

plasmids psPAX2 and pMD2.G (Addgene #12260 and #12259) as well as a lentiviral vector via the calcium phosphate coprecipitation method. After 24 h, target cells were infected in the presence of 8  $\mu$ g/mL polybrene (Sigma). Infected cells were selected for 2 days with 2  $\mu$ g/mL puromycin (Thermo Fisher Scientific).

### MAN2C1 production and enzymatic assays

We transfected HEK293T cells with the different constructs by using JetPEI as DNA transfection reagent. After 48 h, the cells were washed once with cold PBS and harvested in a lysis buffer (HEPES [pH 7.1] 25 mM, PMSF 0.5 mM, antipain/leupeptin 5  $\mu$ g/mL). Cells were subjected to two freeze/thaw cycles in liquid nitrogen and then treated with DNase (100 U per mL of cell extract) for 1 h at 4°C. The cellular extracts were centrifuged at 14,000 g for 15 min at 4°C. The supernatant and the pellet were both kept at -80°C before further experiments.

The mannosidase activity of *MAN2C1* was measured spectrofluorimetrically with 4-methylumbelliferyl  $\beta$ -D-mannopyranoside (4 MUMan) (Sigma-Aldrich M3657) as a substrate. The release of the 4-methylumbelliferone (4 MU) was quantified via excitation and emission wavelengths of 355 nm and 460 nm, respectively. The enzymatic assays were performed in duplicate in 96-well plates at pH 6.5 in MES buffer with 5  $\mu$ L of supernatant from the cell extract and in the presence of 0.5 mM 4 MUMan. The fluorescence of the 4 MU released was measured at 460 nm for the indicated time-points.

## Results

### Clinical features

Family 1 includes individuals 1 and 2 (Table 1 and Figure S1). Two siblings were referred to the genetics clinic for mild global developmental delay. Individual 1 was born at term following vacuum extraction. Biometry and birth parameters were normal. Pregnancy was complicated as a result of gestational diabetes and the finding of a single umbilical artery on fetal ultrasound. Head circumference was normal, but height and weight were above the 95<sup>th</sup> centile as of age 18 and 24 months and beyond, respectively. Renal ultrasound revealed a pyelocaliceal dilatation, which regressed spontaneously. Evaluation at age 7 years showed normal intellectual ability, specific learning difficulties mainly related to expressive language, attention deficit hyperactivity disorder, poor fine motor skills, and mild non-specific dysmorphisms including high forehead, arched eyebrows, short columella, micrognathia, and small ears. Individual 2 was born at term delivery, with normal biometry and birth parameters, after pregnancy complicated by gestational diabetes. At age 8 months, weight and height were normal but her head circumference was above the 95<sup>th</sup> centile. She was diagnosed with mild intellectual disability (global developmental coefficient 67.2 at age 4 years) and autism spectrum disorder. She had mild hearing loss and non-specific dysmorphisms similar to her brother with an additional sandal gap and sacral dimple. Inferior vermis hypoplasia was observed on brain MRI (Figure 2).

**Table 1. Clinical, imaging, and molecular features of the individuals described in this study**

	Family 1		Family 2		Family 3	Family 4
<b>Reference</b>	F9-III:1	F9-III:2	GEF16/274	GEF17/561	D16.0510	PS4501
<b>Sex</b>	male	female	female fetus	male fetus	male	Male
<b>Origin</b>	Portuguese	Portuguese	French	French	Moroccan	American
<b>MAN2C1 genomic variation (GenBank: NM_006715.3)</b>	c.601–2A>G; c.2303G>A	c.601–2A>G; c.2303G>A	c.2612G>C; c.2733_2734del	c.2612G>C; c.2733_2734del	c.607G>A	c.601–2A>G; c.2612G>C
<b>MAN2C1 protein change (GenBank: NP_006706.2)</b>	p.Gly201Profs*10; p.Arg768Gln	p.Gly201Profs*10; p.Arg768Gln	p.Cys871Ser; p.His911Glnfs*67	p.Cys871Ser; p.His911Glnfs*67	p.Gly203Arg	p.Gly201Profs*10; p.Cys871Ser
<b>Inheritance</b>	paternal; maternal	paternal; maternal	paternal; maternal	paternal; maternal	maternal/ paternal	paternal; maternal
<b>Age at last examination</b>	7 years	6 years	28 2/7 GW	29 4/7 GW	18 years	4 years
<b>Macrocephaly</b>	–	+	–	–	+	–
<b>Micro/retrognathia</b>	+	+	+	–	+	+
<b>Dysmorphic features</b>	+	+	+	+	+	+
<b>Tongue hamartoma</b>	–	–	+	+	–	–
<b>Congenital anomalies</b>	pelvicalyceal dilatation	–	–	cleft palate, moderate ureteral dilatation	congenital strabismus	slightly enlarged tongue, joint abnormalities, phimosis
<b>Intellectual disability</b>	–	+	N/A	N/A	+	+
<b>Motor impairment</b>	+	+	N/A	N/A	+	+
<b>Language impairment</b>	+	+	N/A	N/A	+	+
<b>Behavioral problems</b>	+	+	N/A	N/A	+	N/A
<b>Poor social interaction</b>	+	+	N/A	N/A	–	+
<b>Epilepsy</b>	–	–	N/A	N/A	–	N/A
<b>Imaging features</b>						
<b>Brain MRI—age at scan</b>	N/A	5 years	26 2/7 GW	29 4/7 GW	7 years	1 month
<b>Polymicrogyria</b>	N/A	–	–	+	+	+
<b>Heterotopia</b>	N/A	–	+	+	–	–
<b>Ventriculomegaly</b>	N/A	–	+	+	+	–
<b>Callosal anomalies</b>	N/A	–	+	+	+	+
<b>Hypothalamic hamartoma</b>	N/A	–	+	+	–	–
<b>Interhemispheric cysts</b>	N/A	–	–	–	+	–
<b>Cavum vergae</b>	N/A	–	–	–	–	+
<b>Malrotated hippocampus</b>	N/A	–	N/A	N/A	+	N/A
<b>Brainstem hypoplasia</b>	N/A	–	+	+	+	–
<b>Cerebellar hypoplasia</b>	N/A	–	+	–	+	–
<b>Vermis hypoplasia</b>	N/A	+	+	+	+	–

N/A, not applicable; GW, gestational weeks; FMS, fundamental motor skill; pACC, partial agenesis of the corpus callosum; ACC, agenesis of the corpus callosum.

Family 2 includes individuals 3 and 4 (Table 1 and Figure S1). Two pregnancies from the same couple were interrupted respectively at 28 and 29 gestational weeks because of partial agenesis of the corpus callosum, ventriculomegaly, hypothalamic hamartoma, periventricular heterotopia, and vermis hypoplasia at fetal ultrasound.

Fetal brain MRI confirmed these findings and in addition revealed a Z-shaped hypoplastic brainstem (Figure 2). Brain MRI and postmortem examination in individual 3, a boy, showed an irregular cortical surface with deep cortical infolding on the right without evidence of true schizencephaly. Postmortem examination of individual 4, his sister,

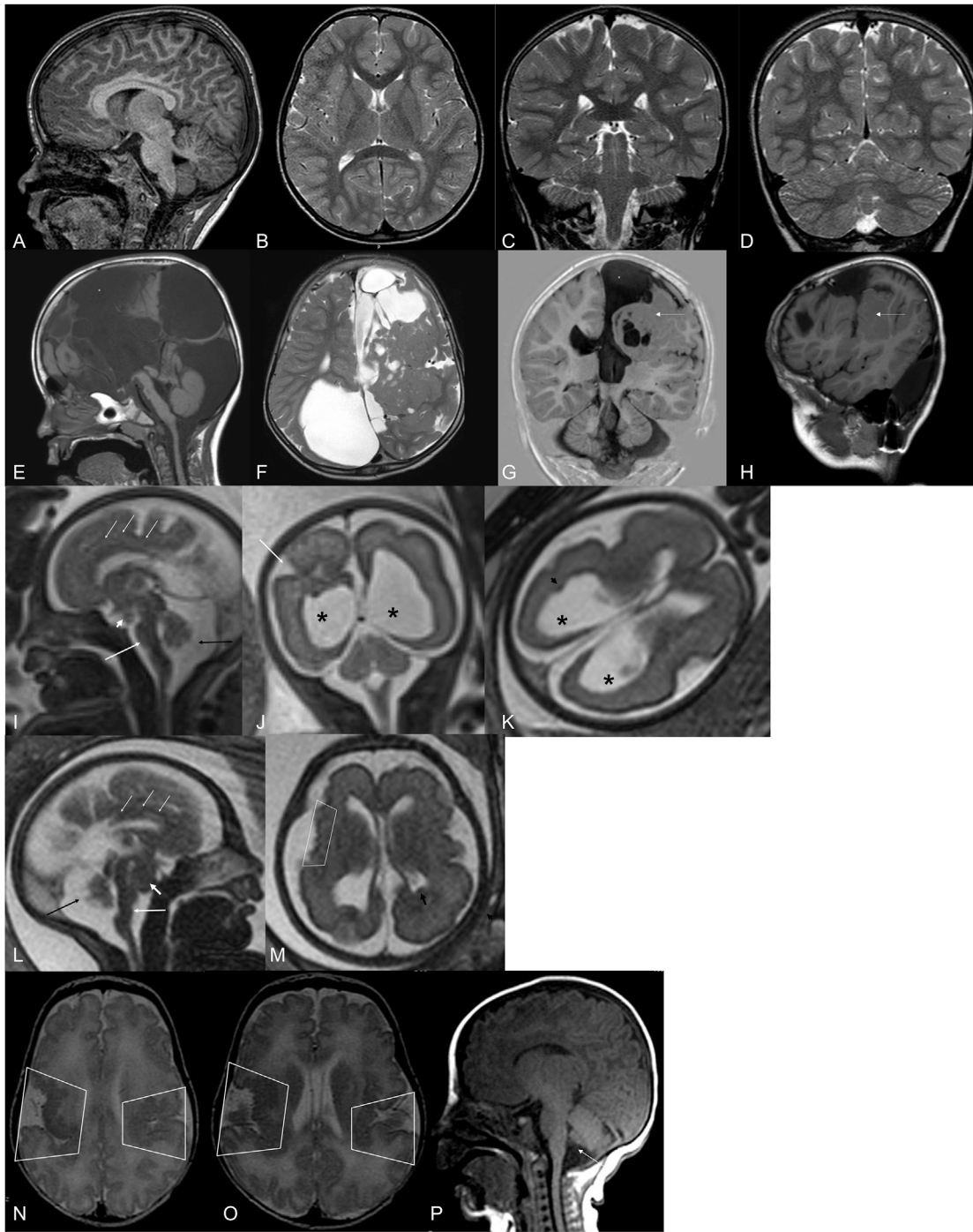


**Figure 2. Imaging features**

Brain MRI of individual 2 at age 5 years (A–D) showing a normal brain structure apart from minor hypoplasia of the inferior cerebellar vermis. Brain MRI of individual 5 at age 7 years (E–H) showing agenesis of the corpus callosum, extensive interhemispheric cysts type 2C (asterisk in E and G), polymicrogyria (arrows in G and H), and brainstem and cerebellar vermis hypoplasia. Brain MRI of individual 3 at 26 gestational weeks (I–K) showing partial agenesis of the corpus callosum (white arrows in I), 3<sup>rd</sup> ventricular floor nodule compatible with hypothalamic hamartoma (white ar in I), cerebellar vermis hypoplasia (black arrow in I), Z-shaped brainstem (solid white arrow in I), irregular deep folding of the right frontal lobe (white arrow in J), bilateral ventricular dilation (asterisk in J), small cerebellum, subependymal heterotopia of the left occipital horn (black ar in K), and bilateral ventricular dilation (asterisks in K). Brain MRI of individual 4 at 29 gestational weeks (L and M) showing partial agenesis of the corpus callosum (white arrows in L), a large nodule in the floor of the 3<sup>rd</sup> ventricle compatible with a hypothalamic hamartoma (white ar in L), hypoplasia of the cerebellar vermis (black arrow in L), a Z-shaped hypoplastic brainstem (solid white arrow in L), bilateral subependymal heterotopia (black ar in M), and a very abnormal bilateral gyration suggestive of polymicrogyria mainly in the fronto-parietal regions (box in M). Brain MRI of individual 6 at 1 month of age (N–P) showing bilateral perisylvian polymicrogyria (box in N and O) as well as diffusely abnormal white matter, thin corpus callosum, and inferior vermis hypoplasia (arrow in P).

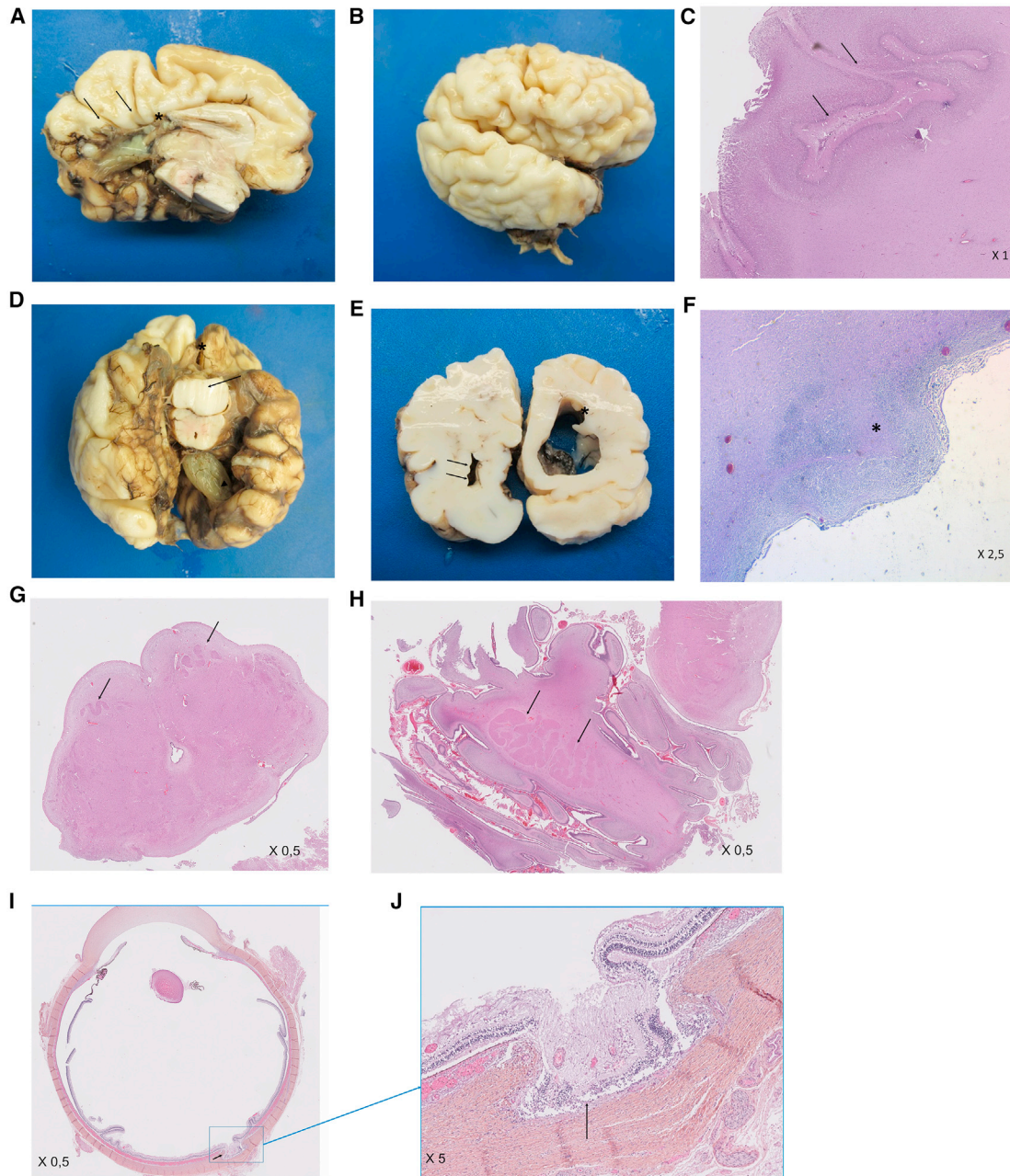


**Figure 3. Brain histology at 30 weeks gestation (individual 4)**

- (A) Left cerebral hemisphere (internal view) with partial posterior corpus callosum agenesis (asterisk) and posterior radial sulci (black arrow).  
 (B) Right cerebral hemisphere with marked gyration with excess of sulci.  
 (C) Right frontal polymicrogyria (black arrows).  
 (D) Lower view of the brain with hypothalamic hamartoma (black arrow), left arhinencephaly (asterisk), and arachnoid cyst (black ar).  
 (E) Right predominantly occipital ventricular dilatation (asterisk) and subependymal nodules (black arrows).  
 (F) Subependymal periventricular heterotopic nodules of gray matter (asterisk).  
 (G) Hypoplastic and fragmented appearance of bulbar olives (black arrows).  
 (H) Fragmented cerebellum deep nuclei (black arrows).  
 (I) Sagittal section of the right eye: retinal coloboma (black arrow).  
 (J) Amplification of retinal coloboma.

revealed hypertelorism, the presence of a retinal coloboma of the right eye, right frontal polymicrogyria, hypoplastic and fragmented bulbar olives, dysplastic deep cerebellar nuclei, and an arachnoid cyst (Figure 3). Both children had a tongue hamartoma. The boy also had a cleft palate.

Family 3 includes individual 5 (Table 1 and Figure S1). The proband is an 18-year-old male who was diagnosed with interhemispheric cysts, agenesis of the corpus callosum, and vermis hypoplasia on fetal ultrasound at 21 gestational weeks. Family history was positive for a simple subarachnoid



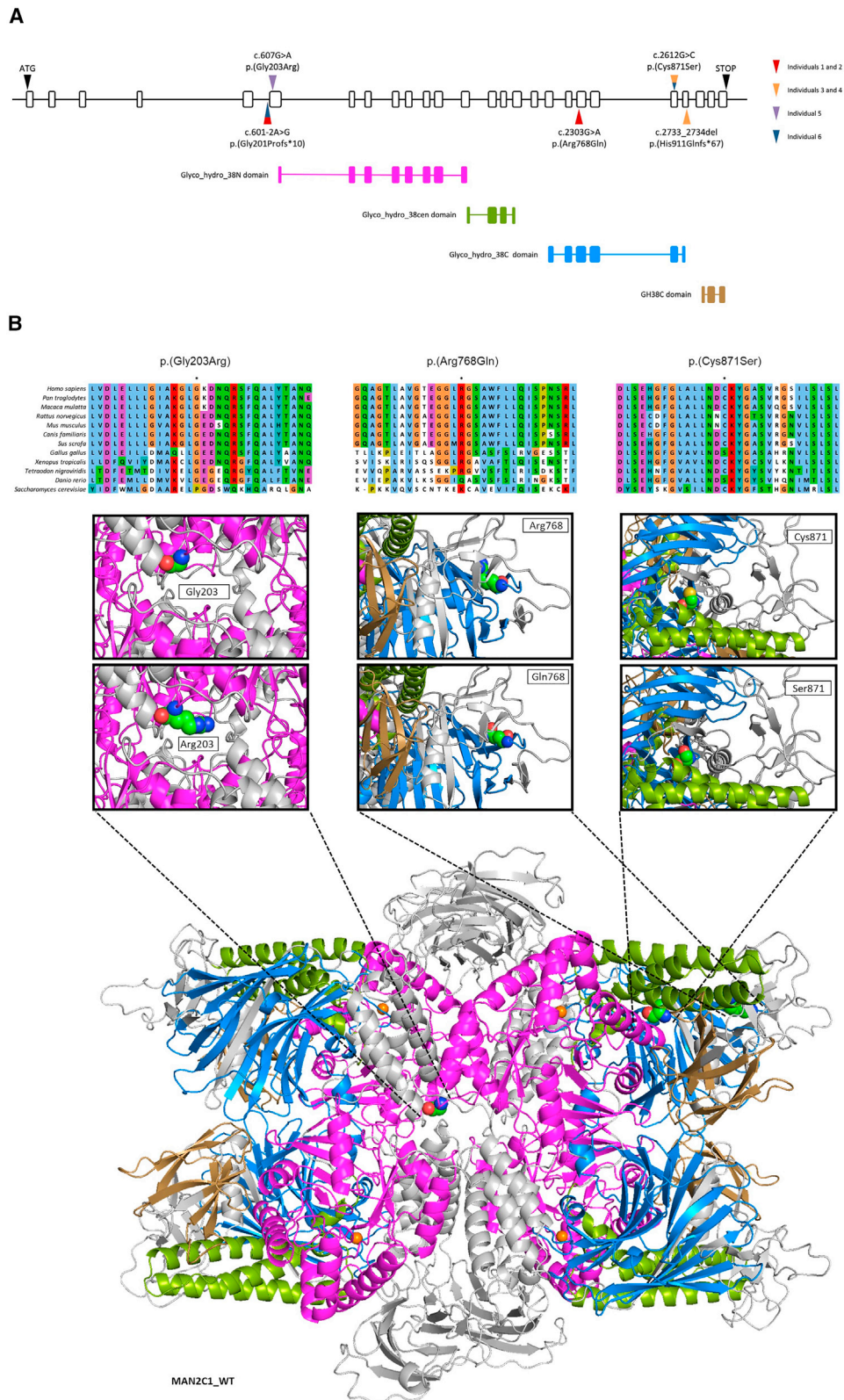


**Figure 4. MAN2C1 variants localization and *in silico* analysis**

(A) Schematic representation of *MAN2C1* variants (GenBank: NM\_006715.3 and NP\_006706.2) along the gene and predicted functional protein domains (not at scale). Exons are represented as white rectangles. Start and stop codons are indicated by black triangles. Each individual is represented by a unique colored triangle: red, 1 and 2; orange, 3 and 4; purple, 5; blue, 6. Domains are represented below respective coding exons, as colored rectangles: pink, glycoside hydrolase family 38 N-terminal domain (Glyco\_hydro\_38N); green, glycoside hydrolase family 38 central domain (Glyco\_hydro\_38cen); blue, glycoside hydrolase family 38 C-terminal domain

(legend continued on next page)

cyst in the father and a paternal cousin with epilepsy for whom no further information was available. The parents lost their first pregnancy at 32 weeks gestation due to chorio-amnionitis. Five siblings are in good health. Brain MRI performed postnatally confirmed the presence of interhemispheric cysts type 2C, extensive subcortical heterotopia, polymicrogyric cortex, complete agenesis of the corpus callosum, malrotation of the hippocampus, and hypoplasia of the brainstem and cerebellum including the cerebellar vermis (Figure 2). At age 7 months, a cysto-peritoneal derivation was performed. He had a single prolonged febrile convulsion at age 20 months. At age 12 years, he was operated on for strabismus. At age 18 years, he is macrocephalic, has retrognathia and a cleft in the left earlobe, can express himself, and counts to 50 and reads simple phrases. There are no behavioral challenges. He has a dystonic quadriplegia, which is more pronounced on the left, but he is able to walk independently.

Family 4 includes individual 6 (Table 1 and Figure S1). The proband is currently a 20-year-old male who was 4 years old at time of last examination. He was born at 36 weeks gestational age by emergency C-section for breech positioning. He was intubated and extubated on day 1 of life, most likely for fluid aspiration or transient tachypnea. His measurements at day 1 of life were within normal limits. Multiple congenital abnormalities were noted shortly after birth: a recessed jaw, mandibular ankylosis, high arched palate, facial asymmetry, slightly enlarged tongue, broad thumbs, ulnar deviation of hands (L > R), unspecified malformation of left hip, and bilateral clubfoot. Clinical examinations were notable for dysphagia with no gag reflex, global developmental delays, hypotonia, nonspecific lower motor neuron disorder, bilateral inversion and hyperextension of knees, and abnormal wrist flexion. He had a brain MRI performed at 1 month, which revealed polymicrogyria involving the right insula and both posterior suprasylvian regions into the posterior frontal lobes (R > L), reduced white matter volume in regions with polymicrogyria, and mild corpus callosum thinning (Figure 2).

### Exome sequencing and gene identification

Exome sequencing was performed independently for each family, and variant filtering following standard strategies, namely allele frequency, presumed inheritance pattern, mutation types, and algorithmic scores for *in silico* assessment of protein function or splicing impact, revealed absence of putative pathogenic variants in known disease genes. Further investigation of bi-allelic variants based on gene biological pathways and CNS expression revealed *MAN2C1* variants (GenBank: NM\_006715.3 and NP\_006706.2) as potentially

disease causing in six individuals belonging to four distinct families collected through GeneMatcher:<sup>26</sup> (1) individuals 1 and 2, c.601–2A>G (p.Gly201Profs\*10) and c.2303G>A (p.Arg768Gln); (2) individuals 3 and 4, c.2612G>C (p.Cys871Ser) and c.2733\_2734del (p.His911Glnfs\*67); (3) individual 5, c.607G>A (p.Gly203Arg) (in homozygosity); and (4) individual 6, c.601–2A>G (p.Gly201Profs\*10) and c.2612G>C (p.Cys871Ser) (Table 1 and Figure 4A). Segregation analysis confirmed that the variants were inherited from healthy parents and that all individuals were either compound heterozygous or homozygous. The parents of individuals 1 and 2 did not have other children. The parents of individuals 3 and 4 had a healthy child born after assisted reproductive technology with oocyte donation. In family 3, the oldest healthy brother and sister did not carry the variant. The parents did not want to have the younger sibling tested. The parents of family 4 did not have any other children. All observed variants have a low population frequency (Table S2) and were absent from gnomAD except the p.Arg768Gln variant for which an allele frequency of 0.0033 was found and five homozygous individuals were identified.

The missense variant c.607G>A, with a CADD score of 23.2, affects a highly conserved nucleotide and amino acid residue, with moderate predicted physicochemical differences, located very close to the glycoside hydrolase family 38 N-terminal domain. Missense variants c.2303G>A and c.2612G>C, located within the glycoside hydrolase family 38 C-terminal domain, have a CADD score of 21.9 and 22.0, respectively. Affected nucleotides are moderately conserved, whereas amino acid residues are highly conserved, with small and moderate predicted physicochemical differences, respectively. *In silico* analysis predicted a splicing acceptor site change due to the canonical splice site c.601–2A>G variant, confirmed by fibroblasts transcript analysis, which revealed the skipping of exon 6, p.Gly201Profs\*10. The frameshift variant, c.2733\_2734del, causes a premature termination codon, reducing the encoded protein by 62 amino acids. We further analyzed the predictive impact of missense variants on the protein structure by three-dimensional modeling (Figure 4B). If *MAN2C1* behaves as its fungal ortholog (*SpAms1*), we can speculate that the replacement of a glycine by an arginine at position 203 will disrupt the formation of the tetramer, as this residue locates between two helix bundles important for inter-subunit interactions.<sup>19</sup> The loss of Arg768, a charged residue, might impair the *MAN2C1* structural stability. Residue 871 allocates in a hydrophobic region showing a striking sequence similarity among species.<sup>19</sup> One can expect that this variant could compromise the inter-subunit interactions.

---

(Glyco\_hydro\_38C); brown, glycoside hydrolase family 38 C-terminal beta sandwich domain (GH38C). Only domains predicted by the InterPro database were included in this figure.

(B) Conservation analysis of amino acids surrounding each missense variant by the Clustal X color code (affected residues are identified above). *In silico* mutagenesis visualization of missense variants following protein structural modeling. *MAN2C1* tetramer structure is represented with the functional domains colored as above (A). Mutated amino acids are superimposed. Further variant description can be found in Table S2.

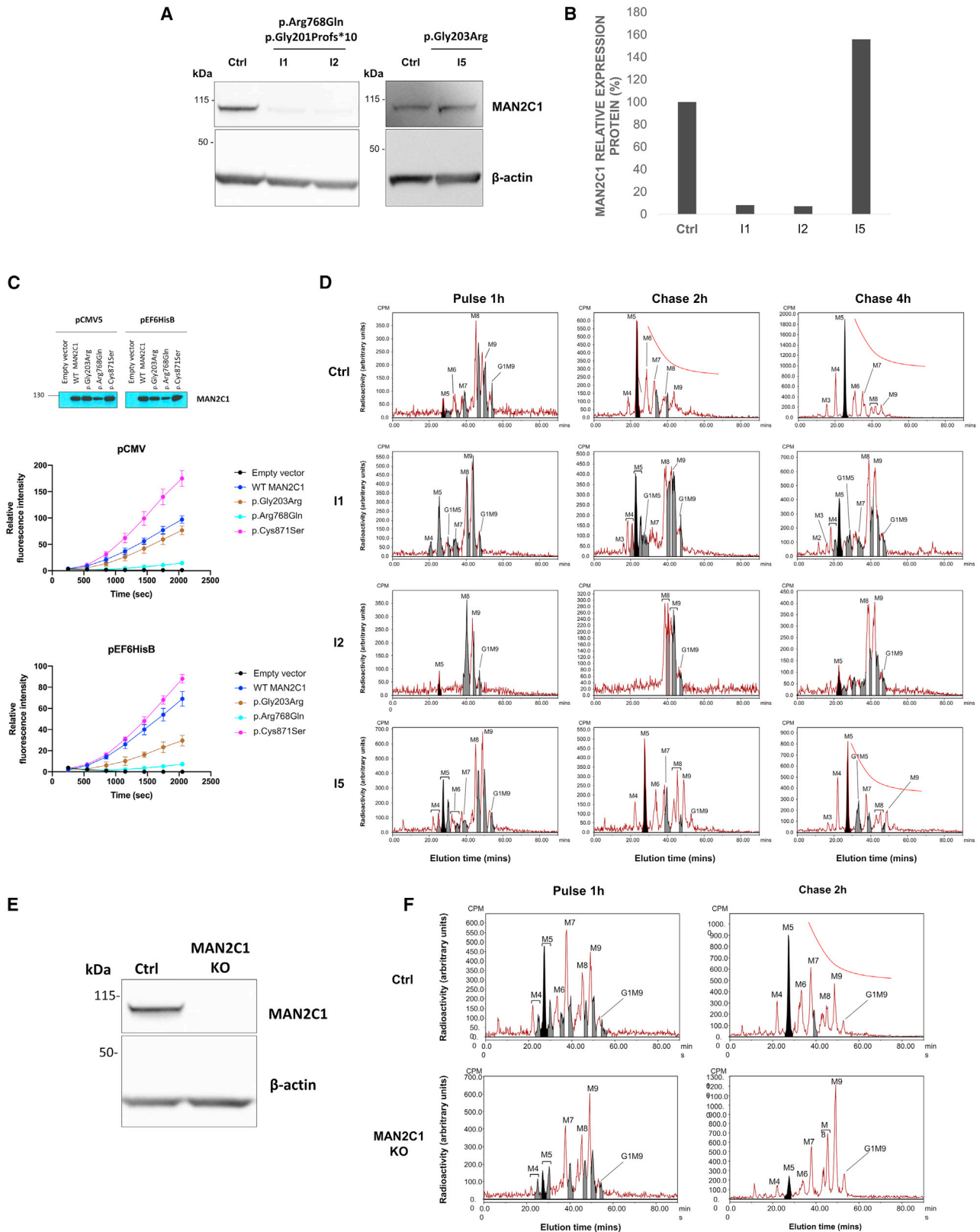


**Figure 5. Individuals with mutations in *MAN2C1* show a defect in fOS processing**

(A) Representative cropped immunoblotting of MAN2C1 in control and proband-derived fibroblasts (I1, I2, and I5).  $\beta$ -actin staining was used as control for gel loading and for the quantification.

(B) Quantification of Man2C1 protein expression in control and proband-derived fibroblasts. Values are means of three independent experiments.

(legend continued on next page)

### Functional validation of *MAN2C1* variants

The impact of the identified variants on the stability of the *MAN2C1* protein was assessed by immunoblot analysis. Primary fibroblast cell lines were available for biochemical analysis for three individuals (1, 2, and 5). When normalized to beta-actin levels, immunoblot analysis showed a 90% reduction in the amount of *MAN2C1* in individuals 1 and 2 when compared to control fibroblasts (Figures 5A and 5B). Interestingly, no significant difference was seen in the steady state *MAN2C1* level in fibroblasts of individual 5 when compared to control fibroblasts. These results show a differential impact of the *MAN2C1* variants on protein abundance. In a first attempt to determine the impact of each identified individual missense variant on *MAN2C1* activity, wild-type (WT) and mutated *MAN2C1* were overexpressed in HEK293 cells with two different expression promoters. Cells were then lysed, and mannosidase activity of crude extracts was measured with 4MUMan as substrate (Figure 5C). Although a slightly reduced abundance for the p.Arg768Gln mutated form can be seen compared to WT in this system, the abundance of the p.Gly203Arg and p.Cys871Ser variants were found to be similar to control. We then tested and compared the mannosidase activities in the HEK293 model. While the p.Gly203Arg mutated form presents a similar activity compared to the WT, the p.Arg768Gln only shows a tiny residual activity, which is consistent with the variant deleteriousness. Very interestingly, the p.Cys871Ser mutated form showed an increased enzyme activity when compared to WT.

### Pathogenic variants in *MAN2C1* cause a defect in fOS processing

As *MAN2C1* activity is involved in fOS processing, we investigated the nature and the fate of the fOS by using HPLC after [2-<sup>3</sup>H]-mannose pulse-chase metabolic labeling experiments in fibroblasts from individuals 1, 2, and 5 compared to control fibroblasts. In control and proband-derived fibroblasts, various high oligomannose Gn<sub>1</sub>- and Gn<sub>2</sub>-species were detected (Figure 5D) Among the fOS present after the pulse period, M<sub>8</sub>Gn<sub>1/2</sub> and M<sub>9</sub>Gn<sub>1/2</sub> species are the most abundant (Table S3). During the chase period, fOSGn<sub>2</sub> (gray peaks) are rapidly converted into fOSGn<sub>1</sub>

(white peaks) by ENGase activity (Figure 5D). The processing of the fOSGn<sub>2</sub> into fOSGn<sub>1</sub> is delayed in individuals 1 and 2 as fOSGn<sub>2</sub> still predominate after 2 h of chase (above 40%) compared to control (9%) (Table S3). However, this delayed processing is not seen for individual 5. The generated fOSGn<sub>1</sub> are the substrates of the *MAN2C1* catalytic activity and are further trimmed into M<sub>5</sub>Gn<sub>1</sub> species during the chase. In control cells and after 2 h of chase, the M<sub>5</sub>Gn<sub>1</sub> species (black peak) (32%) fully accumulates while M<sub>8</sub> and M<sub>9</sub>Gn<sub>1</sub> are barely present (Figure 5D) (Table S3). At 4 h of chase, smaller species (M<sub>3</sub>-M<sub>4</sub>Gn<sub>1</sub>) increase, which are most likely coming from the lysosomal degradation of the cytosolic M<sub>5</sub>Gn<sub>1</sub> species. In all investigated proband-derived fibroblasts, processing of high oligomannose species is delayed (Figure 5D). While some differences can be seen among individuals carrying pathogenic variants in *MAN2C1*, M<sub>8</sub> and M<sub>9</sub>Gn<sub>1/2</sub> species remain over the chase period with a concomitant reduced accumulation of M<sub>5</sub>Gn<sub>1</sub> species arguing for a *MAN2C1* processing defect. This is particularly evident for individual 2 with an absence of M<sub>5</sub>Gn<sub>1</sub> over the chase period (Table S3). In individuals 1 and 5, although a slight accumulation of M<sub>5</sub>Gn<sub>1</sub> species is seen, larger fOS species clearly remain compared to control. Altogether, these results suggest a total or partial loss of function of *MAN2C1* mannosidase activity as a result of p.Arg768Gln and p.Gly203Arg variants.

### *MAN2C1*-KO HAP1 cell line shows a defect in fOS processing

To go further and assess the impact of a lack of *MAN2C1* on fOS processing, we used the *MAN2C1*-KO HAP1 cells. The steady state level of *MAN2C1* was first checked by immunoblotting and showed complete absence of the protein in the KO line compared to the parental cell line (Figure 5E). A [2-<sup>3</sup>H]-mannose pulse-chase metabolic labeling experiment revealed different oligomannose Gn<sub>1</sub>- and Gn<sub>2</sub>-species ranging from M<sub>5</sub> to G<sub>1</sub>M<sub>9</sub> in parental cells after the pulse, and a trimming of the larger fOS species into M<sub>5</sub>Gn<sub>1</sub> species is clearly observed during the chase (Figure 5F). In *MAN2C1*-KO, while larger fOS species (M<sub>7</sub> to M<sub>9</sub>Gn<sub>1</sub>) already predominate after the pulse (Figure 5F), a complete lack of fOS processing during the chase is observed, as no M<sub>5</sub>Gn<sub>1</sub> species are found.

(C) HEK293T were transfected with the indicated constructs driven by two different promoters (pCMV and pEF6HisB) and subjected to *MAN2C1* immunoblot (top). The indicated cells were lysed and then centrifuged, and the supernatant was used to perform enzymatic assays (middle and bottom) with 4-methylumbelliferyl  $\alpha$ -D-mannopyranoside (4MUMan) as substrate. The release of the 4-methylumbelliferone (4MU) was measured at 460 nm for the indicated time-points. Data were normalized to WT *MAN2C1* activity in pCMV. Values are means  $\pm$  SEM of four independent experiments.

(D) fOS HPLC analysis in fibroblast control cell line compared to the different proband-derived fibroblasts (I1, I2, and I5) after 1 h of radioactivity labeling with [2-<sup>3</sup>H] Mannose (left) and after a chase period of 2 h (middle) or 4 h (right). In these chromatograms, fOSGn<sub>2</sub> species are shown in gray and fOSGn<sub>1</sub> in white. The specific product of the *MAN2C1* enzyme, the fOS M<sub>5</sub>Gn<sub>1</sub>, is in black.

(E) Immunoblot analysis of *Man2C1* protein abundance in HAP1 control and KO *MAN2C1* cell lines.  $\beta$ -actin staining was used as control for gel loading and for the quantification.

(F) fOS HPLC analysis in WT-HAP1 compared to the *MAN2C1*-KO HAP1 cells after 1 h of radioactivity labeling with [2-<sup>3</sup>H] mannose (left) and after a chase period of 2 h (right). In these chromatograms, fOSGn<sub>2</sub> species are shown in gray and fOSGn<sub>1</sub> in white. The specific product of the *MAN2C1* enzyme, the fOS M<sub>5</sub>Gn<sub>1</sub>, is in black. G<sub>1</sub>M<sub>9</sub> indicates oligosaccharides possessing one Glc and nine mannose residues. M<sub>9</sub>-M<sub>5</sub> indicates oligosaccharides with five to nine mannose residues. Variants are annotated according the reference sequences GenBank: NM\_006715.3 and NP\_006706.2.

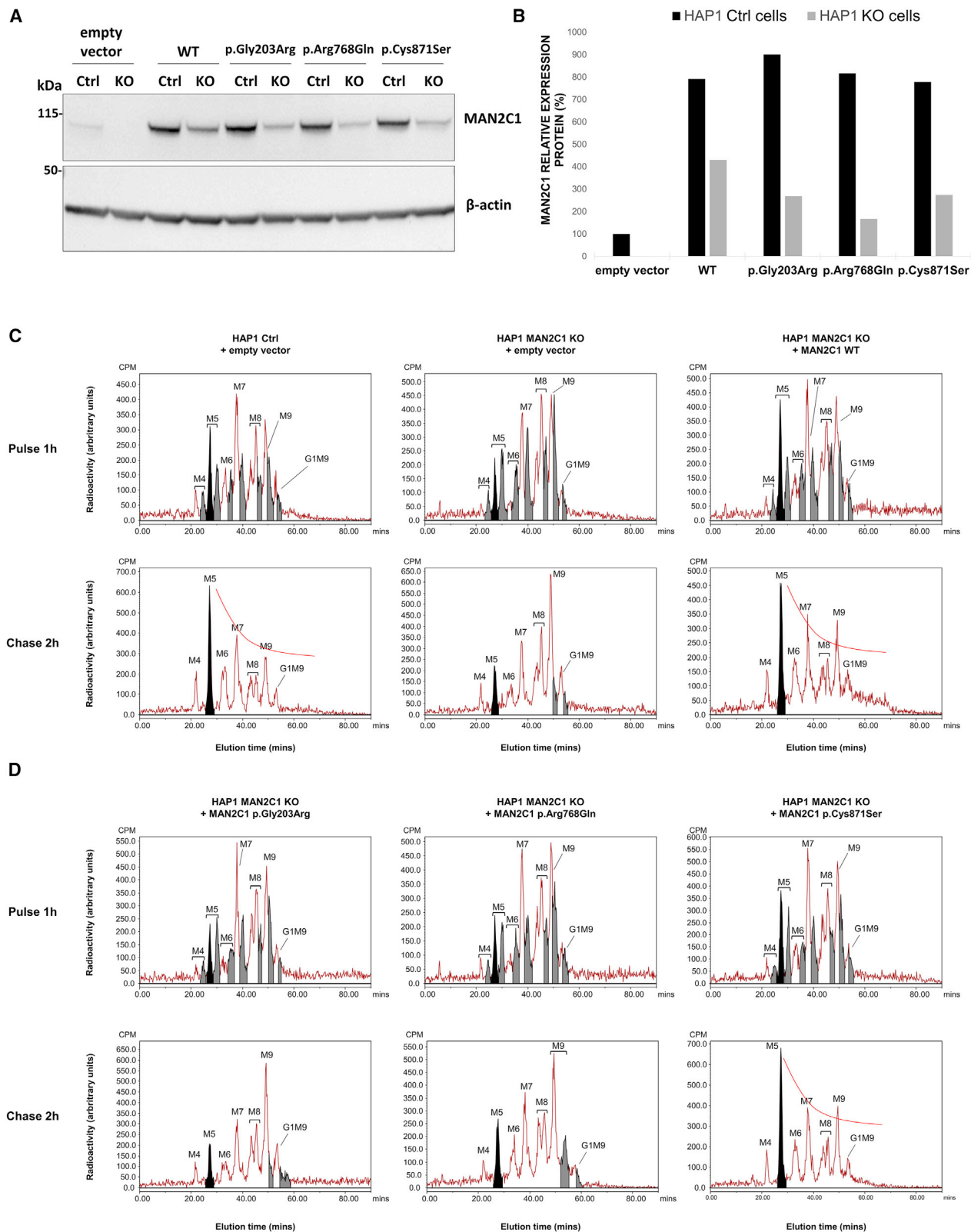


**Figure 6. Pathogenicity of the MAN2C1 variants**

(A) Representative cropped immunoblot of MAN2C1 in HAP1 control and KO MAN2C1 cell lines infected by the empty vector and by different constructs containing WT MAN2C1 or the variant forms of MAN2C1 (p.Gly203Arg, p.Arg768Gln, and p.Cys871Ser) found in MAN2C1-deficient individuals.  $\beta$ -actin staining was used as control for gel loading and for the quantification.

(B) Quantification of MAN2C1 protein abundance in infected HAP1 control and MAN2C1-KO cells. Values are means of three independent experiments.

(legend continued on next page)

### MAN2C1 variants affect fOSs' processing

In order to evaluate the requirement of MAN2C1 in oligosaccharides' processing, we performed genetic complementation of WT-MAN2C1 in MAN2C1-KO HAP1 cells and we reanalyzed fOSs as before. Immunoblot results confirmed the expression of the WT-MAN2C1 in MAN2C1-KO cells (Figures 6A and 6B). Compared to MAN2C1-KO cells, fOS analysis after 2 h of chase in complemented MAN2C1-KO cells shows the processing of larger fOSs into  $M_5Gn_1$  species (black peak). The functional rescue of fOS metabolism via complementation unambiguously demonstrates the involvement of MAN2C1 in this process (Figure 6C). Altogether, these results demonstrate that the absence of MAN2C1 activity affects fOS processing leading to the absence of  $M_5Gn_1$  species and the accumulation of larger fOS  $M_8$  and  $M_9Gn_1$  species.

To assess the effects of the identified human *MAN2C1* variants on mannosidase activity, we complemented MAN2C1-KO HAP1 cells with p.Gly203Arg, p.Arg768Gln, or p.Cys871Ser MAN2C1 variant proteins and subjected them to a [ $2\text{-}^3\text{H}$ ]-mannose pulse-chase experiment. The steady-state protein levels of these variants were first evaluated by immunoblotting, showing a general reduced abundance of the mutant forms when compared to KO cells expressing the MAN2C1-WT (Figure 6A). To circumvent the issue of a differential expression level between the complemented cell lines, we performed the metabolic labeling experiment on control cells complemented with the empty vector and the KO cells complemented with the different variants. No major differences can be seen in fOS analysis after the pulse between the complemented cell lines (Figure 6D). After the chase period, the results are however completely different. A processing of the larger fOS species into  $M_5Gn_1$  species is observed for the p.Cys871Ser MAN2C1-KO complemented cell lines, similar to that observed in the parental HAP1 cells complemented with the empty vector. This finding suggests that this variant does not affect the mannosidase activity. Interestingly, this processing is however not observed in the case of the complementation with the p.Gly203Arg and p.Arg768Gln MAN2C1 mutants, as a significant amount of  $M_7\text{-}M_9Gn_1$  species remains after the chase. A longer chase period does not change the obtained fOS profiles arguing for an accumulation of these species over the time rather than a defect in the flux of these species (data not shown). These results unambiguously demonstrate that the identified *MAN2C1* human

variants c.607G>A (p.Gly203Arg) and c.2303G>A (p.Arg768Gln) impair fOS processing and are pathogenic.

### Discussion

We have identified bi-allelic pathogenic variants in *MAN2C1* in six individuals from four unrelated families as a cause of a congenital disorder of deglycosylation (CDDG) presenting with variable associated phenotypes such as dysmorphic facial features, intellectual disability, and brain anomalies including polymicrogyria, interhemispheric cysts, hypothalamic hamartoma, callosal anomalies, and hypoplasia of brainstem and cerebellar vermis.

Compared to congenital disorders of glycosylation (CDGs), which are a group of inborn errors of metabolism characterized by defects in N-glycoprotein biosynthesis for which more than 140 defects have been reported,<sup>5,6</sup> only one disorder of N-linked deglycosylation has been described so far, the NGLY1-deficiency.<sup>21</sup> The recent identification of EDEM3-deficient individuals has raised interest for this deglycosylation pathway (MIM: 610214)<sup>41</sup>. *MAN2C1* is an enzyme involved in the catabolism of fOSs produced by NGLY1 activity with alpha-mannosidase activity and mitochondria-dependent apoptotic signaling functions.<sup>22</sup> Despite decades of study, the physiological significance of the fOS cytosolic demannosylation is still unknown. In this paper, we connect *MAN2C1* to human disease and provide evidence that two of the three identified missense variants in *MAN2C1* affect the mannosidase activity of this cytosolic enzyme involved in the catabolism of fOSs.

Bi-allelic variants in *MAN2C1* result in highly variable clinical phenotypes (Table 1 and Figure S1). Impact on neurodevelopment ranged from mild language and social impairment in individual 1 to moderate intellectual disability with bilateral cerebral palsy in individual 5. Facial dysmorphisms and congenital anomalies were present in all but varied between individuals. Structural brain anomalies were prominent on brain MRI and/or histology in four of six individuals (Figure 2 and 3) and included polymicrogyria, periventricular heterotopia, hypoplasia of brainstem and cerebellar vermis, malrotated hippocampus, and midline anomalies such as agenesis of the corpus callosum, hypothalamic hamartoma, and interhemispheric cysts type 2C. The cerebral white matter was reduced in individual 6. Interestingly, CNS involvement was also reported in *Man2c1*-deficient mice. Cortical layer

(C) fOS HPLC analysis after 1 h of labeling with [ $2\text{-}^3\text{H}$ ] mannose and after a chase period of 2 h on infected HAP1 cells lines: WT and MAN2C1-KO HAP1 cells infected by empty vector (respectively left and middle) and MAN2C1-KO HAP1 cells complemented with the WT form of MAN2C1 (right).

(D) fOS HPLC analysis after 1 h of radioactivity labeling with [ $2\text{-}^3\text{H}$ ] mannose and after a chase period of 2 h on infected KO MAN2C1 HAP1 cell lines complemented with the different variants from the individuals under study: p.Gly203Arg (left), p.Arg768Gln (middle), and p.Cys871Ser (right). In all chromatograms, fOSGn2 species are shown in gray and fOSGn1 in white; fOS  $M_5Gn_1$ , the specific product of the MAN2C1 enzyme, is in black. In this experiment, *MAN2C1* expression was under the control of the CMV promoter. G1M9 indicates oligosaccharides possessing one glucose and nine mannose residues. M9-M5 indicates oligosaccharides with five to nine mannose residues.

V neurons were degenerated with vacuoles, and white matter lesions characterized by vacuolated oligodendrocytes were abundant.<sup>25</sup> Vacuolization was not observed on brain histology of individuals 3 and 4 at approximately 30 weeks gestation. However, it is not excluded this might be a feature appearing later in life. *Man2c1*-KO mice showed normal appearance and lifespan with the absence of obvious skeletal or behavioral neurological abnormalities. Increased amounts of  $\text{Man}_{9-8}\text{GlcNAc}_1$  mannosylated oligosaccharide species were observed in all analyzed KO tissues as well as an unexplained relatively high glycogen content. An increased staining with mannose-binding lectins, arguing for an accumulation of mannosylated oligosaccharide species, was observed in *Man2c1*-deficient mice compared to controls. The underlying mechanism is not solved yet, but it could well be that the lack of *MAN2C1* activity could interfere with the cytosolic deglycosylation process operated by *NGLY1* and/or the activity of *ENGase*, then disturbing the neuronal proteostasis crucial for normal synaptic physiology. In addition, the loss of *MAN2C1* activity also prevents the release of mannose residues used for GDP-Man synthesis. The relative contribution of mannose salvage pathways to glycosylation is far from being elucidated and it could well be that mannose homeostasis is crucial to sustain physiological processes in certain tissues.

The central question raised by our data is how the brain phenotypes might be explained by the putative loss of function of *MAN2C1* and why such phenotypic variability is observed, ranging from very mild to catastrophic brain malformation. Considering that frameshift variants most likely lead to absent protein, as we did not detect truncated protein with immunoblot analysis of cell lines with frameshift variants (data not shown), a starting point for considering differences between the individuals, and generating hypotheses, comes from analysis of the identified missense variants.

Individual 5 was homozygous for the c.607G>A variant, which led to the most severe brain malformations characterized by polymicrogyria and interhemispheric cysts, classified according to Barkovich et al.<sup>42</sup> as interhemispheric cysts type 2C. To date, no genetic defect underlying this phenotype has been reported. It might therefore be interesting to screen for variants in *MAN2C1* in individuals with this type of brain malformation. With respect to the p.Gly203Arg variant, only a slight decrease in mannosidase activity could be seen with the small substrate 4MUMan, while a clear decrease of p.Gly203Arg activity was found when studying the fate of fOSs in intact cells. This variant may affect the binding of the oligosaccharide in the catalytic site rather than its catalytic activity. In fact, according to the structure of *MAN2C1* fungal ortholog (*ScAms1*),<sup>19</sup> the 203 residue is in a protruding N-terminal tract that could mediate several interactions. Thus, this case illustrates the clearest association of impaired fOS metabolism and cortical malformation.

Individuals 3, 4, and 6 all presented with polymicrogyria, and individuals 3 and 4 had noted periventricular

nodular heterotopia and hypothalamic hamartoma. Each of these individuals was heterozygous for the frameshifting variant p.His911Glnfs\*67 in individuals 3 and 4, or p.Gly201Profs\*10 in individual 6, and the missense p.Cys871Ser variant. As for individuals 1 and 2, a complete loss of function for the frameshift variants is expected because no truncated protein was observed by immunoblot (data not shown). The p.Cys871Ser variant is thus strongly associated with cortical malformation, specifically polymicrogyria, and classified as pathogenic. The observed increased mannosidase activity of this mutation could be interpreted as a gain of function rather than a loss. However, the lack of observed effect of this mutation on fOS processing is not consistent with a gain of function and some possible interpretations can be proposed: (1) the replacement of a cysteine by a serine could allow its phosphorylation by a brain-specific kinase then hampering its mannosidase activity or (2) the p.Cys871Ser variant affects non-mannosidase *MAN2C1* function(s) relevant to brain development. Furthermore, assuming *MAN2C1* adopts a tetrameric structure, as does its fungal ortholog *ScAms1*,<sup>19</sup> stabilized by hydrogen bonds in a highly hydrophobic background, we can speculate that the loss of Cys871 might interfere with inter-subunit interactions or even tetramer formation. Further research is needed to investigate the impact of this variant on *MAN2C1* functions.

Individuals 1 and 2 had relatively mild clinical and brain imaging phenotypes and were compound heterozygous for the p.Gly201Profs\*10 and the p.Arg768Gln variants. The latter strongly affects the *MAN2C1* protein abundance and hence the mannosidase activity, as assessed both by using the synthetic 4 MUMan substrate and by studying the fate of fOSs in intact cells. The relative absence of brain malformations in these individuals compared to the other identified probands is enigmatic and different hypotheses can be proposed. First, it is important to note that individuals 1 and 2 were born from a pregnancy complicated by gestational diabetes. We could tentatively hypothesize that in the case of *MAN2C1* deficiency, high blood glucose levels could act as a protective factor during brain development. Once transported in the cell, glucose is converted to glucose 6-phosphate and fructose-6-phosphate and then to mannose-6 phosphate by phosphomannose isomerase.<sup>43</sup> This enzyme has a very important role in redirecting the fructose-6-phosphate toward mannose metabolism. A higher glucose blood level could increase the mannose-6 phosphate concentration and then the GDP-Man known to be crucial for LLO biosynthesis and the N-glycosylation process. Second, it is also possible that, despite the decreased abundance observed for this variant, the remaining residual non-mannosidase functions are sufficient to protect the brain. A few studies have already highlighted the importance of *MAN2C1* independently of its mannosidase catalytic function in tumorigenesis and malignant transformation.<sup>25</sup> For example, upregulation of *MAN2C1* was observed in human prostate cancer

cells, where MAN2C1 seemed to attenuate PTEN functions by binding to it.<sup>23</sup> It is conceivable that some part of the observed clinical phenotype could originate from PTEN dysfunction. Different neurological features have been reported associated with PTEN defects, including cerebellar dysplastic gangliocytoma, white matter abnormalities, and polymicrogyria. Altogether this further underlines the fact that the severity of the phenotype does not strictly parallel the loss in mannosidase activity and that MAN2C1 may have another function (or other functions), whose perturbations might collectively contribute to the development of the symptoms.

In summary, this study links pathogenic variants in *MAN2C1* to human disease, the second primary defect of N-linked deglycosylation described. Further research is clearly needed to disentangle the complex interrelations between *MAN2C1*, cytosolic fOS species, and brain development.

### Data and code availability

The data supporting the current study have not been deposited in a public database because of privacy and ethical limitations but are available from the corresponding authors on request.

### Supplemental information

Supplemental information can be found online at <https://doi.org/10.1016/j.ajhg.2021.12.010>.

### Acknowledgments

We thank the individuals and their families for their invaluable participation in this work. A.J. and K. Stouffs acknowledge the COST-Action CA16118 (Neuro-MIG-European Network on Brain Malformations). P.J. acknowledges the COST-Action CA16210 (MINDDS—Maximizing Impact of Research in Neurodevelopmental Disorders). F.F. and E.V.S. were supported by the French National Agency (ANR-18-RAR3-0009-01) and the Research Foundation Flanders (FWO), respectively, under the frame of E-Rare-3, the ERA-Net for Research on Rare Diseases (ERA-NET Cofund action no. 64578); F.F. received funding from GLYCOLAB4CDG, an International Associated Laboratory grant from the National Centre for Scientific Research (CNRS); M.C.N. received funding from the Fund for Scientific Research (FRS/FNRS). M.C.N. is a member of Metab-ERN. S.P. was supported by a research fellowship from the Fund for Scientific Research (FNRS, Crédit Chargé de Recherche); P.J., N.M., and A.M.F. are researchers at Unit for Multidisciplinary Research in Biomedicine (UMIB) and ITR—Laboratory for Integrative and Translational Research in Population Health, supported by national funds through the Foundation for Science and Technology (FCT) Portugal (grant numbers UIDB/00215/2020, UIDP/00215/2020, and LA/P/0064/2020, respectively); N.M. was awarded with CHUPorto grant 2016 Departamento de Ensino, Formação e Investigação (DEFI)—CHUPorto. H.Y. is supported by a fellowship from the Research Foundation Marguerite-Marie Delacroix; A.J. is supported by a senior clinical investigator research fellowship of the Research Foundation Flanders (FWO) and is a member of the COST-Action CA16118 Neuro-MIG.

### Declaration of interests

The authors declare no competing interests.

Received: July 19, 2021

Accepted: December 10, 2021

Published: January 18, 2022

### Web resources

Combined annotation-dependent depletion scoring, <https://cadd.gs.washington.edu/score>

gnomAD, [https://gnomad.broadinstitute.org/transcript/ENST00000267978?dataset=gnomad\\_r2\\_1](https://gnomad.broadinstitute.org/transcript/ENST00000267978?dataset=gnomad_r2_1)

HGVS, <https://www.hgvs.org/mutnomen/>

InterPro, <https://www.ebi.ac.uk/interpro/protein/UniProt>

OMIM, <http://www.omim.org/>

PDB, <https://www.rcsb.org/>

PhyloP, <http://compugen.bscb.cornell.edu/phast/help-pages/phyloP.txt>

PyMOL Molecular Graphics System, <https://pymol.org/2/>

Swiss Model Server, <https://swissmodel.expasy.org/>

### References

1. Aebi, M. (2013). N-linked protein glycosylation in the ER. *Biochim. Biophys. Acta* 1833, 2430–2437.
2. Varki, A. (2017). Biological roles of glycans. *Glycobiology* 27, 3–49.
3. Silberstein, S., and Gilmore, R. (1996). Biochemistry, molecular biology, and genetics of the oligosaccharyltransferase. *FASEB J.* 10, 849–858.
4. Freeze, H.H. (2013). Understanding human glycosylation disorders: biochemistry leads the charge. *J. Biol. Chem.* 288, 6936–6945.
5. Ng, B.G., and Freeze, H.H. (2018). Perspectives on Glycosylation and Its Congenital Disorders. *Trends Genet.* 34, 466–476.
6. Péanne, R., de Lonlay, P., Foulquier, F., Kornak, U., Lefeber, D.J., Morava, E., Pérez, B., Seta, N., Thiel, C., Van Schaftingen, E., et al. (2018). Congenital disorders of glycosylation (CDG): Quo vadis? *Eur. J. Med. Genet.* 61, 643–663.
7. Suzuki, T. (2016). Catabolism of N-glycoproteins in mammalian cells: Molecular mechanisms and genetic disorders related to the processes. *Mol. Aspects Med.* 51, 89–103.
8. Suzuki, T. (2007). Cytoplasmic peptide:N-glycanase and catabolic pathway for free N-glycans in the cytosol. *Semin. Cell Dev. Biol.* 18, 762–769.
9. Chantret, I., Fasseu, M., Zaoui, K., Le Bizec, C., Sadou Yayé, H., Dupré, T., and Moore, S.E.H. (2010). Identification of roles for peptide: N-glycanase and endo-beta-N-acetylglucosaminidase (Engase1p) during protein N-glycosylation in human HepG2 cells. *PLoS ONE* 5, e11734.
10. Suzuki, T., Yano, K., Sugimoto, S., Kitajima, K., Lennarz, W.J., Inoue, S., Inoue, Y., and Emori, Y. (2002). Endo-beta-N-acetylglucosaminidase, an enzyme involved in processing of free oligosaccharides in the cytosol. *Proc. Natl. Acad. Sci. USA* 99, 9691–9696.
11. Harada, Y., Hirayama, H., and Suzuki, T. (2015). Generation and degradation of free asparagine-linked glycans. *Cell. Mol. Life Sci.* 72, 2509–2533.
12. Moore, S.E., and Spiro, R.G. (1994). Intracellular compartmentalization and degradation of free polymannose oligosaccharides



- released during glycoprotein biosynthesis. *J. Biol. Chem.* 269, 12715–12721.
13. Moore, S.E. (1998). Transport of free polymannose-type oligosaccharides from the endoplasmic reticulum into the cytosol is inhibited by mannosides and requires a thapsigargin-sensitive calcium store. *Glycobiology* 8, 373–381.
  14. Suzuki, T., Hara, I., Nakano, M., Shigeta, M., Nakagawa, T., Kondo, A., Funakoshi, Y., and Taniguchi, N. (2006). Man2C1, an  $\alpha$ -mannosidase, is involved in the trimming of free oligosaccharides in the cytosol. *Biochem. J.* 400, 33–41.
  15. Chantret, I., and Moore, S.E.H. (2008). Free oligosaccharide regulation during mammalian protein N-glycosylation. *Glycobiology* 18, 210–224.
  16. Kmićik, D., Herman, V., Stroop, C.J., Michalski, J.C., Mir, A.M., Labiau, O., Verbert, A., and Cacan, R. (1995). Catabolism of glycan moieties of lipid intermediates leads to a single Man5GlcNAc oligosaccharide isomer: a study with permeabilized CHO cells. *Glycobiology* 5, 483–494.
  17. Duvet, S., Labiau, O., Mir, A.M., Kmićik, D., Krag, S.S., Verbert, A., and Cacan, R. (1998). Cytosolic deglycosylation process of newly synthesized glycoproteins generates oligomannosides possessing one GlcNAc residue at the reducing end. *Biochem. J.* 335, 389–396.
  18. Hunter, S., Apweiler, R., Attwood, T.K., Bairoch, A., Bateman, A., Binns, D., Bork, P., Das, U., Daugherty, L., Duquenne, L., et al. (2009). InterPro: the integrative protein signature database. *Nucleic Acids Res.* 37, D211–D215.
  19. Zhang, J., Wang, Y.-Y., Du, L.-L., and Ye, K. (2020). Cryo-EM structure of fission yeast tetrameric  $\alpha$ -mannosidase Ams1. *FEBS Open Bio* 10, 2437–2451.
  20. Lam, C., Ferreira, C., Krasnewich, D., Toro, C., Latham, L., Zein, W.M., Lehky, T., Brewer, C., Baker, E.H., Thurm, A., et al. (2017). Prospective phenotyping of NGLY1-CDDG, the first congenital disorder of deglycosylation. *Genet. Med.* 19, 160–168.
  21. Enns, G.M., Shashi, V., Bainbridge, M., Gambello, M.J., Zahir, F.R., Bast, T., Crimian, R., Schoch, K., Platt, J., Cox, R., et al. (2014). Mutations in NGLY1 cause an inherited disorder of the endoplasmic reticulum-associated degradation pathway. *Genet. Med.* 16, 751–758.
  22. Wang, L., and Suzuki, T. (2013). Dual functions for cytosolic  $\alpha$ -mannosidase (Man2C1): its down-regulation causes mitochondria-dependent apoptosis independently of its  $\alpha$ -mannosidase activity. *J. Biol. Chem.* 288, 11887–11896.
  23. He, L., Fan, C., Kapoor, A., Ingram, A.J., Rybak, A.P., Austin, R.C., Dickhout, J., Cutz, J.-C., Scholey, J., and Tang, D. (2011).  $\alpha$ -Mannosidase 2C1 attenuates PTEN function in prostate cancer cells. *Nat. Commun.* 2, 307.
  24. Paciotti, S., Persichetti, E., Klein, K., Tasegian, A., Duvet, S., Hartmann, D., Gieselmann, V., and Beccari, T. (2014). Accumulation of free oligosaccharides and tissue damage in cytosolic  $\alpha$ -mannosidase (Man2c1)-deficient mice. *J. Biol. Chem.* 289, 9611–9622.
  25. Cáceres, A., Esko, T., Pappa, I., Gutiérrez, A., Lopez-Espinosa, M.-J., Llop, S., Bustamante, M., Tiemeier, H., Metspalu, A., Joshi, P.K., et al. (2016). Ancient Haplotypes at the 15q24.2 Microdeletion Region Are Linked to Brain Expression of MAN2C1 and Children's Intelligence. *PLoS ONE* 11, e0157739.
  26. Sobreira, N., Schiettecatte, F., Valle, D., and Hamosh, A. (2015). GeneMatcher: a matching tool for connecting investigators with an interest in the same gene. *Hum. Mutat.* 36, 928–930.
  27. den Dunnen, J.T., and Antonarakis, S.E. (2001). Nomenclature for the description of human sequence variations. *Hum. Genet.* 109, 121–124.
  28. den Dunnen, J.T., and Antonarakis, S.E. (2000). Mutation nomenclature extensions and suggestions to describe complex mutations: a discussion. *Hum. Mutat.* 15, 7–12.
  29. Karczewski, K.J., Francioli, L.C., Tiao, G., Cummings, B.B., Alfoldi, J., Wang, Q., Collins, R.L., Laricchia, K.M., Ganna, A., Birnbaum, D.P., et al. (2020). The mutational constraint spectrum quantified from variation in 141,456 humans. *Nature* 581, 434–443.
  30. Kircher, M., Witten, D.M., Jain, P., O'Roak, B.J., Cooper, G.M., and Shendure, J. (2014). A general framework for estimating the relative pathogenicity of human genetic variants. *Nat. Genet.* 46, 310–315.
  31. Reese, M.G., Eeckman, F.H., Kulp, D., and Haussler, D. (1997). Improved splice site detection in Genie. *J. Comput. Biol.* 4, 311–323.
  32. Cooper, G.M., Stone, E.A., Asimenos, G., Green, E.D., Batzoglu, S., Sidow, A.; and NISC Comparative Sequencing Program (2005). Distribution and intensity of constraint in mammalian genomic sequence. *Genome Res.* 15, 901–913.
  33. UniProt Consortium (2019). UniProt: a worldwide hub of protein knowledge. *Nucleic Acids Res.* 47 (D1), D506–D515.
  34. Yates, A.D., Achuthan, P., Akanni, W., Allen, J., Allen, J., Alvarez-Jarreta, J., Amode, M.R., Armean, I.M., Azov, A.G., Bennett, R., et al. (2020). Ensembl 2020. *Nucleic Acids Res.* 48 (D1), D682–D688.
  35. Larkin, M.A., Blackshields, G., Brown, N.P., Chenna, R., McGettigan, P.A., McWilliam, H., Valentin, F., Wallace, I.M., Wilm, A., Lopez, R., et al. (2007). Clustal W and Clustal X version 2.0. *Bioinformatics* 23, 2947–2948.
  36. Waterhouse, A.M., Procter, J.B., Martin, D.M.A., Clamp, M., and Barton, G.J. (2009). Jalview Version 2—a multiple sequence alignment editor and analysis workbench. *Bioinformatics* 25, 1189–1191.
  37. Grantham, R. (1974). Amino acid difference formula to help explain protein evolution. *Science* 185, 862–864.
  38. Berman, H.M., Battistuz, T., Bhat, T.N., Bluhm, W.F., Bourne, P.E., Burkhardt, K., Feng, Z., Gilliland, G.L., Iype, L., Jain, S., et al. (2002). The Protein Data Bank. *Acta Crystallogr. D Biol. Crystallogr.* 58, 899–907.
  39. Schwede, T., Kopp, J., Guex, N., and Peitsch, M.C. (2003). SWISS-MODEL: An automated protein homology-modeling server. *Nucleic Acids Res.* 31, 3381–3385.
  40. Rigsby, R.E., and Parker, A.B. (2016). Using the PyMOL application to reinforce visual understanding of protein structure. *Biochem. Mol. Biol. Educ.* 44, 433–437.
  41. Polla, D.L., Edmondson, A.C., Duvet, S., March, M.E., Sousa, A.B., Lehman, A., Niyazov, D., van Dijk, F., Demirdas, S., van Slegtenhorst, M.A., et al. (2021). Bi-allelic variants in the ER quality-control mannosidase gene EDEM3 cause a congenital disorder of glycosylation. *Am. J. Hum. Genet.* 108, 1342–1349.
  42. Barkovich, A.J., Simon, E.M., and Walsh, C.A. (2001). Callosal agenesis with cyst: a better understanding and new classification. *Neurology* 56, 220–227.
  43. Ichikawa, M., Scott, D.A., Losfeld, M.-E., and Freeze, H.H. (2014). The metabolic origins of mannose in glycoproteins. *J. Biol. Chem.* 289, 6751–6761.